Nonequilibrium scalings of turbulent wakes

M. Obligado, T. Dairay, and J. C. Vassilicos*
Department of Aeronautics, Imperial College London, London, United Kingdom
(Received 12 January 2016; published 16 August 2016)

Nonequilibrium turbulent wake scalings are not the preserve of irregular (fractal-like/multiscale) plates but appear to be universal, as they also hold for regular plates over a very substantial downstream distance.

DOI: 10.1103/PhysRevFluids.1.044409

The most basic and arguably most important property that any theory or model of turbulence must predict is the mean flow profile. A model or theory of turbulence which can do this for a wide range of turbulent flows on the basis of only few fundamental and robust assumptions is still lacking. However, in the case of canonical boundary-free turbulent shear flows such as turbulent jets, wakes, and mixing layers, one can predict how the mean velocity difference and the size of the mean flow profile evolve with streamwise distance on the basis of two cornerstone assumptions [1]. These two assumptions may not be sufficient for a complete mean flow profile prediction, but they do lead to some of its most important aspects. The first assumptions is self-preservation of one-point turbulence statistics and the second is the scaling of the turbulence dissipation rate (see [1–3]).

The high Reynolds number scaling of the turbulence dissipation rate traditionally used is the one consistent with the Richardson-Kolmogorov equilibrium cascade. The resulting streamwise developments (power laws of streamwise distance) of the mean velocity difference and the size of the mean flow profile are in many classical textbooks (e.g., [1,2,4]) for many canonical boundary-free turbulent shear flows. Recently, however, a new high Reynolds number dissipation law has been found in decaying and in forced periodic turbulence [5] and in near-field grid-generated decaying turbulence for many different types of grids (see [6]). The region where this nonequilibrium dissipation law holds can be long, depending on the turbulence-generating grid.

Before proceeding to the implications of this nonequilibrium dissipation law for mean flow profiles, we recall the reasons (see [6]) why this dissipation law is termed "nonequilibrium." In a Richardson-Kolmogorov equilibrium cascade of turbulent kinetic energy the turbulent dissipation rate instantaneously equals the rate with which energy is fed into the cascade at the large energy-containing scales. This rate scales with the kinetic energy and size of these large scales at the instant considered and is independent of viscosity. Hence the turbulence dissipation must scale in the same way. Any different scaling of the turbulence dissipation must therefore characterize an instantaneous imbalance between dissipation and the rate with which energy is fed into the cascade at the large scales and it must therefore be a nonequilibrium scaling. This argument has a mathematical analog in terms of the generalized Karman-Howarth equation which can be found in Ref. [6] and which is based on setting the unsteady term in this equation to zero (for equilibrium). Of course, there are also spatial inhomogeneity terms in this equation which are negligible if small enough scales are considered in flows which are not extremely inhomogeneous (i.e., if inertial range scales are smaller than the length scale characterizing statistical inhomogeneity). Goto and Vassilicos [7] considered the Lin equation, which is the Fourier equivalent of the Karman-Howarth equation when the turbulence is statistically homogeneous, and ran direct numerical simulations (DNS) of periodic turbulence to confirm the above. The Lin equation holds in this context and the DNS of [7] did indeed confirm that the turbulence dissipation and the large-scale energy flux (which in their context corresponds to the rate at which energy is fed into the cascade at the large scales) scale differently. The reason for this difference lies in the cascade time-lag which is why instantaneous equilibrium is absent.

*Corresponding author: j.c.vassilicos@imperial.ac.uk

They found the well-known classical scaling for the large-scale energy flux but they also found the same nonequilibrium scaling for the turbulence dissipation that previous studies had found in other unsteady turbulent flows [5,6,8].

Nedić *et al*. [9] used this nonequilibrium dissipation law in conjunction with the self-preservation hypothesis to derive mean flow profile scalings for nonequilibrium axisymmetric turbulent wakes. Specifically, their nonequilibrium predictions for the streamwise evolution (along x) of the centerline mean velocity deficit u_0 and the wake width δ are

$$u_0(x) = AU_\infty[(x - x_0)/\theta]^{-1}, \tag{1}$$

$$\delta(x) = B\theta[(x - x_0)/\theta]^{1/2}, \tag{2}$$

where A and B are dimensionless constants, U_∞ is the incoming free-stream velocity, θ the momentum thickness, and x_0 a virtual origin. The momentum thickness θ is defined by $\theta^2 = \frac{1}{U_\infty^2}\int_0^\infty U_\infty(U_\infty - U)r\,dr$ which is constant with x, and the wake's width is here characterized by the integral wake's width δ defined by $\delta^2(x) = \frac{1}{u_0}\int_0^\infty (U_\infty - U)r\,dr$ where U is the mean streamwise velocity. The wake-generating object is characterized by a length scale L_b. The equilibrium predictions for axisymmetric turbulent wakes (see [1,3]) are

$$u_0(x) = AU_\infty[(x - x_0)/\theta]^{-2/3}, \tag{3}$$

$$\delta(x) = B\theta[(x - x_0)/\theta]^{1/3}. \tag{4}$$

The nonequilibrium predictions (1) and (2) and the classical predictions (3) and (4) rely on axisymmetry of turbulence wake statistics, self-preservation of $U_\infty - U$, turbulent kinetic energy K, Reynolds shear stress R_{xr} and turbulence dissipation ε, and on a scaling law for the centerline turbulence dissipation. Both sets of predictions are obtained from the Reynolds averaged streamwise momentum and turbulent kinetic energy equations, leading to a closed set of equations for $u_0(x)$ and $\delta(x)$. This set of equations is different for different dissipation scalings leading to (3) and (4) in the classical case and to (1) and (2) in the nonequilibrium case (see [8] for details).

Nedić *et al*. [9] confirmed predictions (1) and (2) experimentally using hot wire anemometry (HWA) in the range $5L_b < x \leqslant 50L_b$ on mean flow profiles of axisymmetric and self-preserving turbulent wakes of thin plates with irregular edges placed normal to the incoming free stream (in which case L_b is the square root of the plate's frontal area $\mathcal{A}$). Irregular edges increase the velocity deficit without increasing $\mathcal{A}$, hence one can better measure velocity deficits without reducing the streamwise range of measurements in the wind tunnel's test section. However, it remains a key open question whether the nonequilibrium scalings reported in Ref. [9] are specific to plates with irregular edges or are universal and therefore also valid for regular plates.

In this paper we report HWA and direct numerical simulation (DNS) results for turbulent wakes of regular plates which demonstrate the validity of the nonequilibrium dissipation scalings. We then present a careful analysis of mean flow profile data which shows that the nonequilibrium wake scalings (1) and (2) are consistent with this data. The nonequilibrium turbulence dissipation law is $\varepsilon_0 = C_\varepsilon K_0^{3/2}/\delta$, where K_0 is centerline turbulent kinetic energy, ε_0 is centerline turbulence dissipation, and C_ε is a dimensionless coefficient which is not constant as in equilibrium turbulence but proportional to the ratio of two Reynolds numbers, $\mathrm{Re}_G/\mathrm{Re}_L$. $\mathrm{Re}_G \equiv U_\infty L_b/\nu$ is a global Reynolds number determined by the inlet conditions and $\mathrm{Re}_L \equiv \sqrt{K_0}\delta/\nu$ is a local Reynolds number dependent on x (ν stands for the kinematic viscosity of the flow).

The experiments were run in a low background turbulence wind tunnel with $\sim 91 \times 91$ cm^2 test section of length 4.25 m. The experimental setup is as in Ref. [9]. The plate has square peripheries and has a reference length $L_b = 64$ mm with thickness 1.25 mm. It is suspended normal to the laminar free stream in the test section center using four 0.5 mm diameter piano wires. U_∞ was fixed at 10 m/s, the velocity fluctuations around the mean being below 0.1% for an empty test section.

HWA measurements were taken downstream of the wake generator using a Dantec Dynamics 55P01 hot-wire probe, driven by a Dantec StreamLine CTA system. The Pt-W wire was 5 μm in diameter, 3 mm long, with 1.25 mm sensing length. The wake centerline was found by searching the maximum of the velocity deficit u_0 through successive iterations and with cross-wire checks described below. To obtain mean turbulent wake profiles, the probe was traversed at each streamwise location $x/L_b = 10,15,20,25,30,35,40,45,50$ in 10 mm vertical intervals normal to the streamwise x axis between $y = -250$ mm and $y = 250$ mm. The acquisition time was 60 s with 20 kHz sampling rate (each profile acquisition took about 1 hour of measurements). Two calibrations (beginning and end) were made for each profile, while temperature was monitored not to exceed a variation of 0.2 °C. The results reported here correspond to the lower half of the profiles measured, while the whole profile was used to check the positioning of the center of the wake.

The axisymmetry of the flow was studied by taking radial-polar profiles at $x/L_b = 10$ and 30. Measurements for these profiles were taken at 8 radial positions (5, 10, 20, 35, 50, 75, 100, and 150 cm) and 25 polar angles equispaced between $-\pi$ and π with the same wire. Taking into account the centerline position, this gives 193 points at each streamwise position. Each point measurement was acquired for 30 s at 20 kHz and a new calibration was taken each 30 min with the same procedure as the one described above for temperature variations.

Finally, a Dantec Dynamics 55P51 x-wire probe (with the same wires as for our single-wire probe) was used for centerline measurements. At each centerline position, 30 min of data were acquired at 20 kHz. A new calibration was performed at every centerline position and temperature variations were monitored as explained above.

The x-wire measurements were used to calculate the centerline kinetic energy by assuming axisymmetry, i.e., $K_0 = 0.5(\langle u_x'^2\rangle + 2\langle u_r'^2\rangle)$ where u_x' and u_r' are streamwise and radial fluctuating velocities.

The turbulent energy dissipation was only estimated on the centerline from single-wire measurements acquired over 30 min with 20 kHz sampling rate. It was calculated as $\varepsilon_{\rm iso} = \int 15\nu k_1^2 E_{11} dk_1$ where $E_{11}(k_1)$ is the one-dimensional (1D) power spectrum and $k_1 = 2\pi f/U$, f being a Fourier frequency in Hz. We therefore assume local isotropy at the centerline and we use the Taylor hypothesis (the turbulence intensity based on the local mean flow velocity is always below, and in most cases much smaller than 12%). The validity of the local isotropy was established by our DNS with results very similar to those in Ref. [8].

The acquisition time of the centerline single-wire measurements being 30 min, on the order of 100 000 integral time scales at each streamwise position were recorded, allowing good large-scale resolution. The Kolmogorov frequency was always smaller than half our sampling frequency (which is 20 kHz) except at the position closest to the plate ($x/L_b = 10$) where it was 11 kHz. At this position where our Kolmogorov microscale η is at its smallest, $\eta = 140$ μm, but it grows with streamwise distance to reach $\eta \approx 0.42$ mm at $x/L_b = 50$. We checked that the main contribution to the integral $\int 15\nu k_1^2 E_{11} dk_1$ comes in all our cases from wave numbers $k_1\eta \leqslant 0.5$ and that variations to the dissipation spectrum at wave numbers higher than $k_1\eta = 0.5$ modeled by various exponential shapes imply variations in our estimates of $\varepsilon_{\rm iso}$ of less than 6%.

To simulate a spatially evolving wake generated by a square plate, the high-order finite difference code INCOMPACT3D was used to solve the incompressible Navier-Stokes equations [10,11]. Numerical methodology, spatial resolution, and computational domain are the same as in Ref. [8]. The modeling of the square plate is performed by an immersed boundary method, following a procedure proposed by [12]. Inflow and outflow boundary conditions are assumed in the streamwise direction, with a uniform fluid velocity U_∞ without turbulence as inflow condition and a 1D convection equation as outflow condition. Boundary conditions in the two spanwise directions are periodic. The computational domain $L_x \times L_y \times L_z = 120L_b \times 15L_b \times 15L_b$ is discretized on a Cartesian regular grid of $n_x \times n_y \times n_z = 3841 \times 480 \times 480$ points. In terms of Kolmogorov microscale η, the spatial resolution is at worst $\Delta x \approx 7\eta$ (at $x \approx 7L_b$ where the turbulence is at its most intense) and at best $\Delta x \approx 0.8\eta$ (at the end of the computational domain where the turbulence has decayed). The lateral dimensions of the computational domain have been chosen as in the experiments. Because of the very big size

TABLE I. Coefficient of variance of U/U_∞ and R_{xx}/U_∞^2 at $x/L_b = 10$ and $x/L_b = 30$ obtained with HWA and DNS. Bracketed values are maximum coefficients of variance across all radial distances.

	$x/L_b = 10$		$x/L_b = 30$	
	U/U_∞	R_{xx}/U_∞^2	U/U_∞	R_{xx}/U_∞^2
HWA	1.17(1.36)	3.0 (3.76)	0.30(0.60)	4.25(6.73)
DNS	0.17(0.31)	1.33 (3.49)	0.07(0.12)	1.61(2.32)

of these massively parallel simulations, $\mathrm{Re}_G = 5000$, i.e., 8 times smaller than in our wind tunnel experiments. Details about the code INCOMPACT3D can be found in Refs. [10,11], and in Ref. [13] for its massively parallel version.

It has been verified that the momentum conservation $(\theta/\delta)^2 = u_0/U_\infty$ holds for all streamwise positions for both DNS and HWA. The momentum thickness is well converged and has a constant value of $\theta = 19.7$ mm for the HWA measurements and $\theta = 19.2$ mm for the DNS.

The scalings (1) and (2) follow from three premises, the first being axisymmetry of turbulent wake statistics. We therefore check the axisymmetry of the flow at $x = 10/L_b$ and $x/L_b = 30$ by scrutinising the radial-polar profiles of normalized centerline mean flow velocity and streamwise Reynolds stress acquired with HWA and DNS. This is achieved by computing the mean values of the coefficient of variance

$$c_v(x,r) \equiv 100\frac{\sqrt{(1/N_\varphi)\sum_\varphi [S(x,r,\varphi) - \langle S\rangle(x,r)]^2}}{\langle S\rangle(x,r)}, \tag{5}$$

where N_φ is the number of azimuthal angles and S stands for mean flow U or streamwise Reynolds stress R_{xx}. The streamwise variations of the radially averaged coefficient of variance $\overline{c_v}(x) \equiv (1/N_r)\sum_r c_v(x,r)$ (computed for $r \in [0; L_b]$) are shown in Table I. It can be appreciated that the averaged and maximum values of c_v are very low, remaining always below 1.5% for U/U_∞ and below 7% for R_{xx}/U_∞^2. Thus, the flow is already axisymmetric at $x = 10L_b$.

The second important property on which the scalings (1) and (2) rely is self-preservation of $U_\infty - U$, R_{xr}, K, and ε (see [8] and note that our DNS of the present flow showed negligible differences between ε calculated from its exact definition and ε calculated from Taylor's isotropic expression which follows from local isotropy). In Fig. 1(a) we plot $f(r/\delta) = \frac{U_\infty - U}{U_\infty - U_0}$ versus r/δ for different streamwise distances x. HWA and DNS profiles of $f(r/\delta)$ at various x collapse very well, and the other profiles obtained with DNS (not accessible with our HWA) are also extremely well collapsed. Our DNS evidence shows that the required quantities are all self-preserving for $x/L_b \geqslant 15$.

The third pivotal property behind the scalings (1) and (2) is the nonequilibrium turbulence dissipation scaling. This scaling requires high Reynolds numbers, specifically Taylor length Reynolds numbers Re_λ larger than about 200 [5,6]. The local Reynolds number $\mathrm{Re}_L = \sqrt{K_0}\delta/\nu$ remains always above 2000 and Re_λ clearly above 200 in our HWA measurements [Figs. 2(a) and 2(b)]. We therefore concentrate our attention on our HWA measurements of C_ε.

In Figs. 3(a) and 3(b) we plot $C_\varepsilon^{\mathrm{Eq}} = \varepsilon_0\delta/K_0^{3/2}$ and $C_\varepsilon^{\mathrm{Non-Eq}} = \varepsilon_0(\mathrm{Re}_L/\mathrm{Re}_G)\delta/K_0^{3/2}$ respectively. A Richardson-Kolmogorov equilibrium cascade is consistent with $C_\varepsilon^{\mathrm{Eq}} = \mathrm{const}$ [5,6], which is clearly not observed in our flow between $x = 10L_b$ and $x = 50L_b$. However, the nonequilibrium scaling $C_\varepsilon^{\mathrm{Noneq}} = \mathrm{const}$ observed in various unsteady turbulent flows [5,6] is also observed here. While $C_\varepsilon^{\mathrm{Eq}}$ increases by more than 75% from $x = 10L_b$ to $x = 50L_b$, $C_\varepsilon^{\mathrm{Noneq}}$ remains quite constant with $C_\varepsilon^{\mathrm{Noneq}} = 0.0272 \pm 0.0015$. Our high Reynolds number HWA data strongly support the presence of the nonequilibrium dissipation law in the turbulent wake of a regular plate.

We now complement our centerline dissipation measurements (see Fig. 3) with further HWA data. In Fig. 4(a) we plot a cross section of ε at $x/L_b = 10$. It can be seen that ε is already axisymmetric

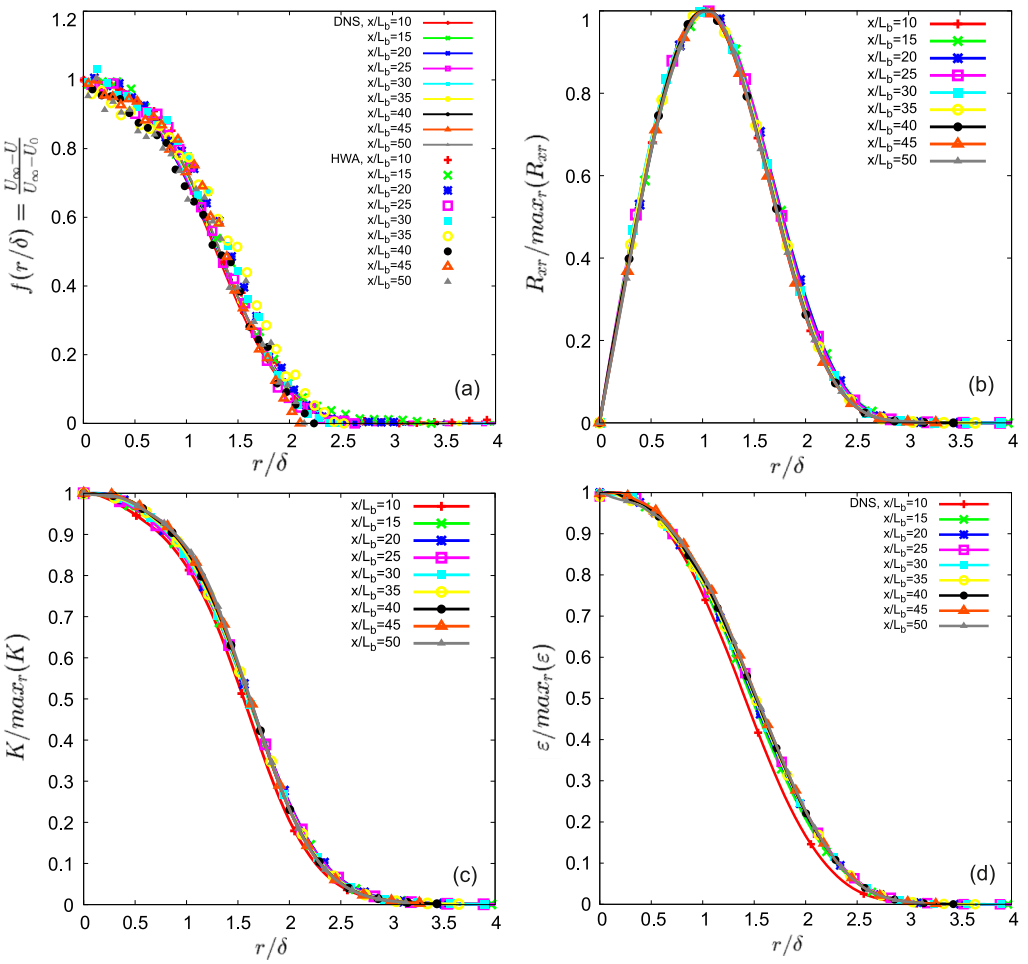

FIG. 1. Mean flow profiles at different streamwise distances plotted using similarity scalings (a). Markers stand for HWA measurements while lines stand for DNS data. Profiles of R_{xr} (b), K (c), and ε (d) normalized by the maximum radial value at different streamwise distances versus r/δ for DNS only.

at $x/L_b = 10$ (with a mean coefficient of variance $\overline{c_v} = 5$) without any sign of the large-scale wake flow periodicity which one might be tempted to somehow relate to the nonequilibrium behavior of the turbulence dissipation. Furthermore, Fig. 4(b) supports the view that ε is self-similar from $x/L_b = 15$ onwards as shown by our DNS data in Fig. 1(d). Self-similarity implies that $\varepsilon(x,r)$ at $r = 0$ has to decay like $\varepsilon(x,r)$ at $r = \delta$ (or any other constant multiple of δ). This is demonstrated in Fig. 4(b), suggesting that the presence of nonequilibrium scalings can also be seen off centerline given that the turbulent kinetic energy K is also self-similar [see Fig. 1(c)].

The three pillars supporting (1) and (2) (axisymmetry, self-preservation, and nonequilibrium) having been established, it remains to show that (1) and (2) are consistent with the data. In Figs. 5(a)–5(d) the normalized velocity deficit and wake width are plotted in two ways: one which returns a linear dependence in the case of equilibrium turbulence corresponding to (3) and (4) and one which returns a linear dependence in the case of nonequilibrium turbulence corresponding to (1) and (2). Both sets of exponents return acceptable linearizations of the data. This explains why previous studies (e.g., [9] and references therein) have concluded that the mean velocity deficit and wake width of axisymmetric turbulent wakes of regular objects scale in the classical equilibrium

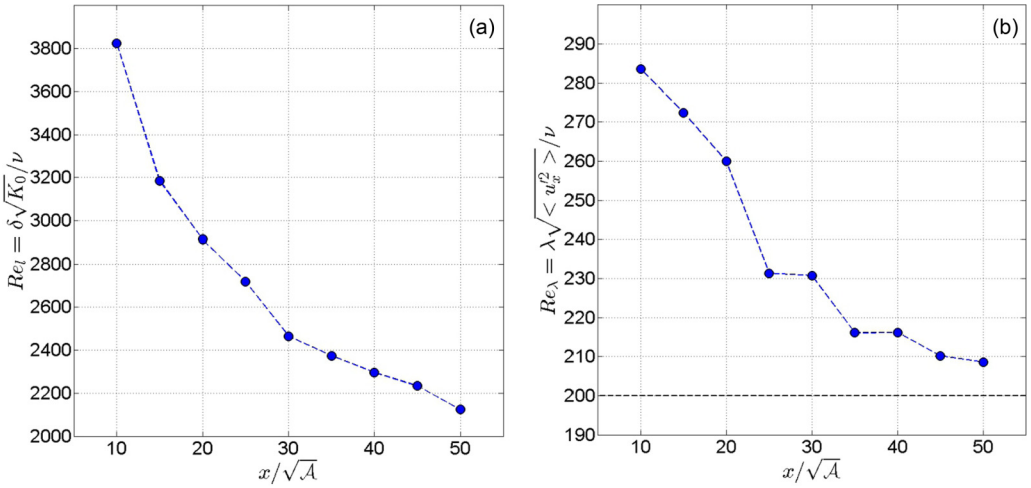

FIG. 2. Streamwise variation of local Reynolds number $\mathrm{Re}_L = \sqrt{K_0}\delta/\nu$ (a). Streamwise variation of Reynolds number $\mathrm{Re}_\lambda = \sqrt{\langle u_x'^2\rangle}\lambda/\nu$ based on the Taylor microscale $\lambda = \sqrt{15\nu\langle u_x'^2\rangle/\varepsilon_{\mathrm{iso}}}$ (b). The black dashed line represents the lower limit $\mathrm{Re}_\lambda = 200$ for nonequilibrium scalings proposed in Ref. [5].

way described in various textbooks (e.g., [1,2,4]). The advantage we have relative to these studies is that we know the nonequilibrium dissipation law and its validity in some flows (including, as shown here, the present flow) and that this new dissipation law implies (1) and (2) if self-similarity and axisymmetry are satisfied, and we have demonstrated in this work that they are. The difficulty with regular plates compared to the fractal-like irregular-edge plates of [9] and [8] is that the velocity deficits are much smaller, causing the exponents obtained from best fits of data to be extremely sensitive to measurement uncertainties and therefore also to the fitting method used. Having demonstrated axisymmetry, self-similarity, and nonequilibrium dissipation, we now propose a fitting method which can return the resulting nonequilibrium scalings (1) and (2). We also make the point that, in cases such as the present one, it is impossible to discriminate between equilibrium and nonequilibrium scalings by only fitting mean centerline velocity and wake width data.

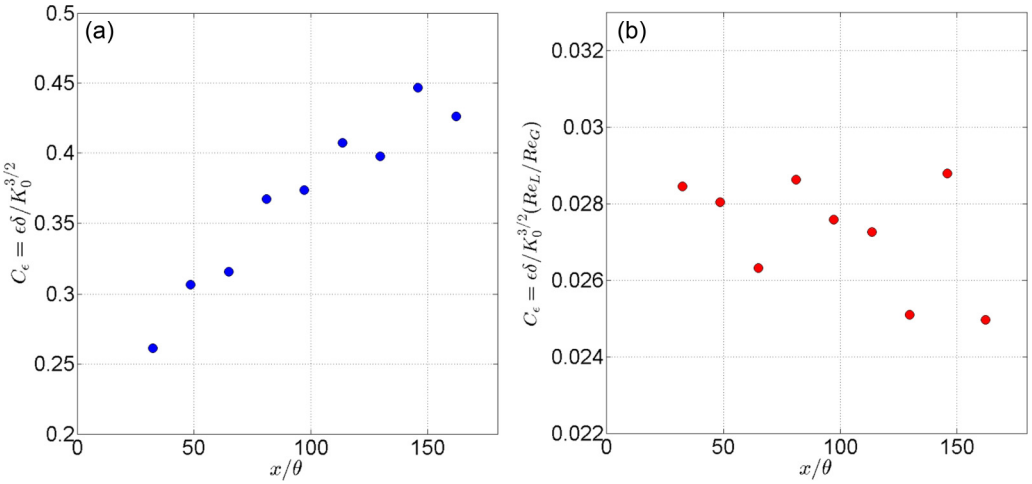

FIG. 3. Equilibrium dissipation coefficient $C_\varepsilon^{\mathrm{Eq}} = \varepsilon_0\delta/K_0^{3/2}$ (a). Nonequilibrium dissipation coefficient $C_\varepsilon^{\mathrm{Noneq}} = \varepsilon_0\delta/K_0^{3/2}(\mathrm{Re}_L/\mathrm{Re}_G)$ (b).

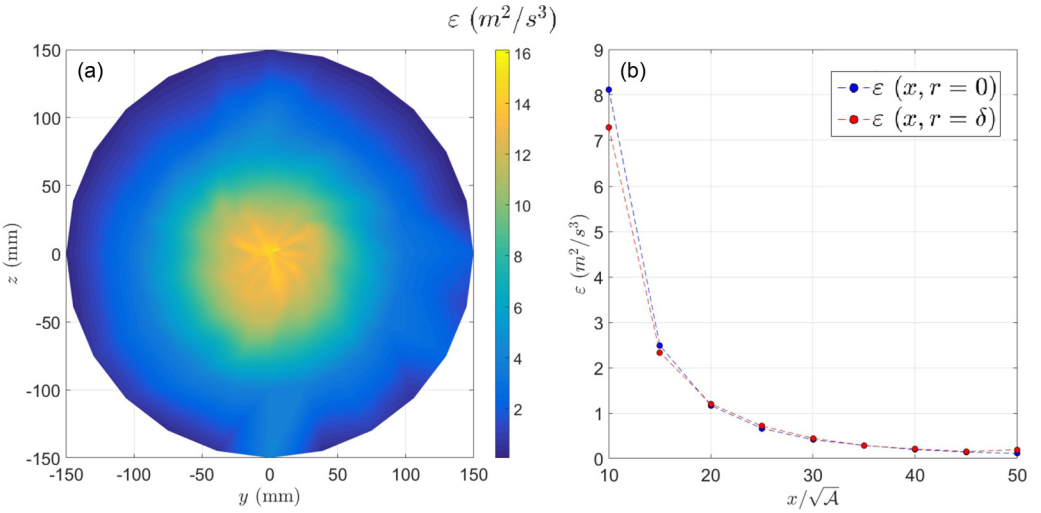

FIG. 4. Cross section of ε at $x/L_b = 10$ (a). Comparison of the streamwise evolution of ε at $r = 0$ (blue line) and $r = \delta$ (red line) (b). ε was estimated using the same method as in Fig. 3.

We start by writing

$$(u_0/U_\infty)^{-1/\alpha} = A^{-1/\alpha}\frac{x - x_{0\alpha}}{\theta} = A^{-1/\alpha}\frac{x}{\theta} - A^{-1/\alpha}\frac{x_{0\alpha}}{\theta}, \tag{6}$$

$$(\delta/\theta)^{1/\beta} = B^{1/\beta}\frac{x - x_{0\beta}}{\theta} = B^{1/\beta}\frac{x}{\theta} - B^{1/\beta}\frac{x_{0\beta}}{\theta} \tag{7}$$

and search for exponents α and β which return a linear regression coefficient R^2 closest to 1. An important advantage of this method is that it determines the exponents α and β independently of virtual origin. Once α and β are known, the linear fits (6) and (7) give the constants A and B and the virtual origin x_0. Figure 6 shows the coefficient R^2 as function of α for the velocity deficit equation (6) and as function of β for the wake width equation (7). There is a well resolved maximum in both cases and both maxima are at values of α and β which are very close to the nonequilibrium predictions $\alpha = 1$ and $\beta = 1/2$. The equilibrium predictions ($\alpha = 2/3$ and $\beta = 1/3$) are visibly far from the maxima.

The optimum exponents obtained in the way just described and the other parameters in equations (6) and (7) turn out to be $A = 4.07 \pm 0.22$, $\alpha = 1.000 \pm 0.001$, $B = 0.494 \pm 0.014$, and $\beta = 0.501 \pm 0.001$. Note that our fitting method returns similar virtual origins from both (6) and (7) independently ($x_0/\theta \approx -6.20 \pm 5.82$). Table II lists the values of R^2 for the best fit, the equilibrium, and the nonequilibrium predictions and confirms that nonequilibrium scalings are very close to the optimal fits. However, it is also clear from Figs. 5 and 6 and Table II that the equilibrium predictions can also fit the mean flow deficit and wake width data with comparable, if only marginally less good, quality of fit. Furthermore these data are such that a different fitting method can lead to a different conclusion; for example the fitting method of [9] gives a marginal preference for (3) and (4) when applied to our data. However both fitting methods return (1) and (2) unequivocally when

TABLE II. Values of R^2 obtained for different sets of fits.

Plate	Equilibrium	Nonequilibrium	Best fit
R^2_α	0.969	0.980	0.980
R^2_β	0.967	0.977	0.977

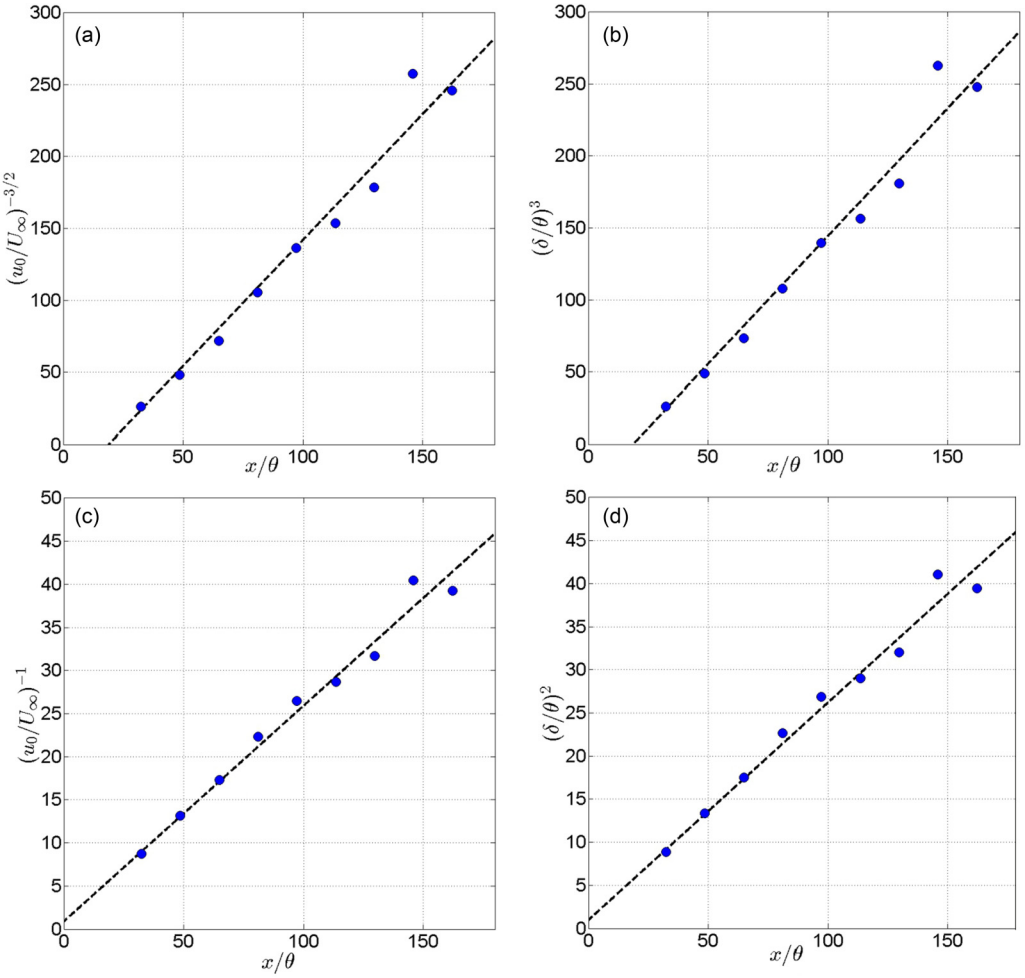

FIG. 5. Normalized velocity deficit linearized according to equilibrium scalings, $(u_0/U_\infty)^{-3/2}$, as a function of x/θ (a). Normalized wake width linearized according to equilibrium scalings, $(\delta/\theta)^3$, as a function of x/θ (b). Same parameters linearized according to nonequilibrium scalings: $(u_0/U_\infty)^{-1}$ for the normalized velocity deficit (c) and $(\delta/\theta)^2$ for the normalized wake width (d).

applied to the mean flow deficit and wake width data of the fractal-like plates of [9], and this is because the fractal-like plates of [9] return sufficiently higher mean flow velocity deficits which can be measured more accurately. Hence, without our dissipation, self-similarity, and axisymmetry plots, we are unable to chose between (1) and (2) on the one hand and (3) and (4) on the other for our regular plate. Our observation that fits such as those of Fig. 6 cannot be conclusive on their own if the velocity deficit is not high enough can explain previous inconclusive measurements in the literature, which always used regular wake generators and did not take dissipation measurements.

These points of caution having been made, the fits in Figs. 5 and 6 and Table II do nevertheless show that our experimental measurements are compatible with the proposed nonequilibrium scaling laws (1) and (2). Our observations of axisymmetry, self-similarity, and nonequilibrium dissipation scaling imply that the scaling laws (3) and (4), even if apparently compatible with our wake deficit and width data, are inconsistent with the totality of our data. The fitting method that we propose is one which can return wake width and deficit scalings that are consistent with the rest of our data, ε data in particular.

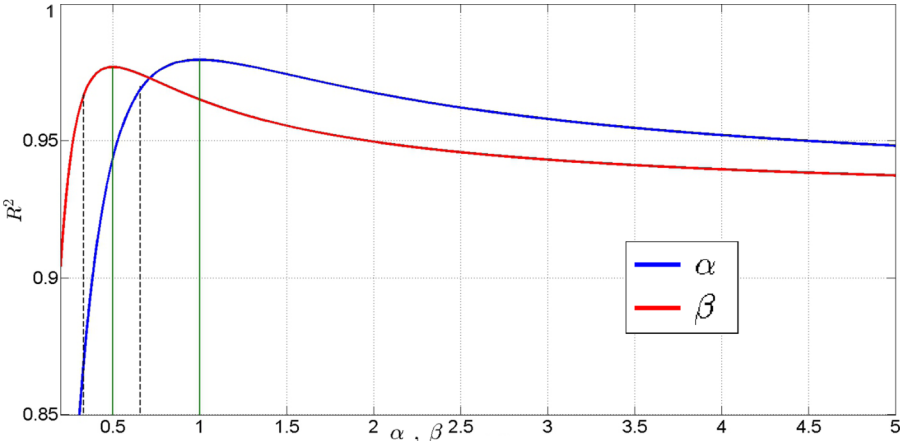

FIG. 6. Linear regression coefficient R^2 as function of scaling exponents for u_0/U_∞ (blue line) and δ/θ (red line). The black vertical dotted lines locate the equilibrium scaling exponents while the green vertical lines locate the nonequilibrium ones.

In conclusion, the nonequilibrium laws $\varepsilon_0 \sim \frac{\mathrm{Re}_G}{\mathrm{Re}_L} K_0^{3/2}/\delta$, (1) and (2) appear to be universal. This conclusion is supported by the ubiquity of the nonequilibrium dissipation law [5,6], which is further supported by our present dissipation measurements and by recent simulations of turbulent wakes of spheres [14], which also support (1) and (2). Of course, more research is needed to cover a broader range of flows, inlet geometries, and Reynolds numbers to clearly establish the universality class where the nonequilibrium dissipation law holds. Much further downstream where Re_λ drops below about 100 and where experiments and simulations of other flows suggest the emergence of the classical dissipation law (see [4] and [14]), we might expect to find classical wake laws in agreement with the simulations of [15]. However, it is an open question whether a turbulence which has not achieved equilibrium at high upstream values of Re_λ can achieve equilibrium much further downstream where the values of Re_λ have very significantly dropped. Future experiments which resolve the far downstream wake and also achieve much higher global Reynolds numbers Re_G should help to shed light on this question.

We were supported by an ERC Advanced grant (2013-2018) awarded to J.C.V. The simulations were performed at the PDC Centre for High Performance Computing (KTH Royal Institute of Technology) with resources provided by the DECI-11 project FRAPLAWI (EC funding RI-312763) and at the SuperMUC supercomputer at Leibniz-Rechenzentrum (Leibniz Supercomputing Centre) with resources awarded by PRACE. We acknowledge the UK Turbulence Consortium (EPSRC research grant EP/L000261/1) for UK supercomputing resources.

[1] A. A. Townsend, *The Structure of Turbulent Shear Flow* (Cambridge University Press, Cambridge, UK, 1976).

[2] H. Tennekes and J. L. Lumley, *A First Course in Turbulence* (MIT Press, Cambridge, MA, 1972).

[3] W. K. George, The self-preservation of turbulent flows and its relation to initial conditions and coherent structures, in *Advances in Turbulence*, edited by W. K. George and R. Arndt (Hemisphere, New York, 1989), pp. 39–73.

[4] S. B. Pope, *Turbulent Flows* (Cambridge University Press, Cambridge, UK, 2000).

[5] S. Goto and J. C. Vassilicos, Energy dissipation and flux laws for unsteady turbulence, Phys. Lett. A **379**, 1144 (2015).
[6] J. C. Vassilicos, Dissipation in turbulent flows, Annu. Rev. Fluid Mech. **47**, 95 (2015).
[7] S. Goto and J. C. Vassilicos, Local equilibrium hypothesis and taylors dissipation law, Fluid Dyn. Res. **48**, 021402 (2016).
[8] T. Dairay, M. Obligado, and J. C. Vassilicos, Non-equilibrium scaling laws in axisymmetric turbulent wakes, J. Fluid Mech. **781**, 166 (2015).
[9] J. Nedić, J. C. Vassilicos, and B. Ganapathisubramani, Axisymmetric Turbulent Wakes with New Nonequilibrium Similarity Scalings, Phys. Rev. Lett. **111**, 144503 (2013).
[10] S. Laizet and E. Lamballais, High-order compact schemes for incompressible flows: A simple and efficient method with quasi-spectral accuracy, J. Comput. Phys. **228**, 5989 (2009).
[11] S. Laizet, E. Lamballais, and J. C. Vassilicos, A numerical strategy to combine high-order schemes, complex geometry and parallel computing for high resolution DNS of fractal generated turbulence, Comput. Fluids **39**, 471 (2010).
[12] P. Parnaudeau, J. Carlier, D. Heitz, and E. Lamballais, Experimental and numerical studies of the flow over a circular cylinder at Reynolds number 3900, Phys. Fluids **20**, 085101 (2008).
[13] S. Laizet and N. Li, Incompact3d: A powerful tool to tackle turbulence problems with up to $O(10^5)$ computational cores, Int. J. Numer. Methods Fluids **67**, 1735 (2011).
[14] M. B. de Stadler, N. R. Rapaka, and S. Sarkar, Large eddy simulation of the near to intermediate wake of a heated sphere at Re = 10,000, Int. J. Heat Fluid Flow **49**, 2 (2014).
[15] J. A. Redford, I. P. Castro, and G. N. Coleman, On the universality of turbulent axisymmetric wakes, J. Fluid Mech. **710**, 419 (2012).